

A semiclassical study of the generic spin model on a triangular lattice

Yao-Dong Li¹ and Gang Chen^{2,3*}

¹*School of Computer Science, Fudan University, Shanghai, 200433, People's Republic of China*

²*State Key Laboratory of Surface Physics, Center for Field Theory and Particle Physics, Department of Physics, Fudan University, Shanghai 200433, People's Republic of China and*

³*Collaborative Innovation Center of Advanced Microstructures, Fudan University, Shanghai, 200433, People's Republic of China*

(Dated: December 8, 2024)

Motivated by the recent experiments on the quantum spin liquid candidate material YbMgGaO_4 , we study the generic spin model that describes the interaction between the spin-orbit-entangled Kramers' doublet local moments on the triangular lattice. We combine the Luttinger-Tisza method, the classical Monte Carlo simulation, and the self-consistent spin-wave theory to analyze the generic spin Hamiltonian. Taking two coupling constants from the experiments, we obtain a classical phase diagram that includes the 120° state and two stripe ordered phases. We find the frustration is strong and significantly suppresses the ordering temperature in the regions close to the phase boundary between different ordered phases. Going beyond the semiclassical treatment, we include the quantum fluctuations within a self-consistent spin-wave analysis and find the strong quantum fluctuation in the frustrated regions can melt the magnetic order. Our results provide a guidance for the numerical search of possible quantum spin liquid ground state of the generic spin model and are relevant for the magnetic properties of other triangular spin-1/2 magnets.

Introduction.—Quantum spin liquid (QSL) is a novel quantum state of matter in which strong quantum fluctuation suppresses the conventional magnetic order down to zero temperature [1, 2]. The theoretical understanding of QSLs is very well-established with exactly solvable models that supports QSL ground states [3] as well as formal classifications of QSLs on various lattices [4]. A more recent theory argued that the ground state of a spin-orbit coupled insulator with odd number of electrons per unit cell must be exotic [5]. This result suggests that strong spin-orbit coupled insulators can in principle be the hosts for QSLs. Nevertheless, the existence of QSLs in realistic physical systems is still elusive despite one decade of active search [1, 2]. Recently, a new material YbMgGaO_4 is proposed to be a candidate system for QSLs [6], which might point to a confluence between the experiments and the fundamental theories. This material remains disordered down to 60mK [6, 7]. The Yb^{3+} ion contains thirteen $4f$ electrons and experiences very strong atomic spin-orbit coupling, it was thus proposed that YbMgGaO_4 is the first QSL candidate system with strong spin-orbit coupling and odd number of electrons per unit cell [6].

In YbMgGaO_4 , the Yb^{3+} ions form a perfect triangular lattice. The interlayer separation between nearby Yb triangular layers is 8.4\AA and is much larger than the intralayer Yb lattice constant that is 3.4\AA . Because the Yb $4f$ electron is very localized spatially, one can safely neglect the interlayer coupling and focus on the intralayer coupling between the Yb moments.

The strong spin-orbit coupling of the Yb $4f$ electrons entangles the orbital angular momentum ($L = 3$) with the spin angular momentum ($s = 1/2$), giving rise to a total angular momentum $J = 7/2$ that is further split into four Kramers' doublets by the D_{3d} crystal electric

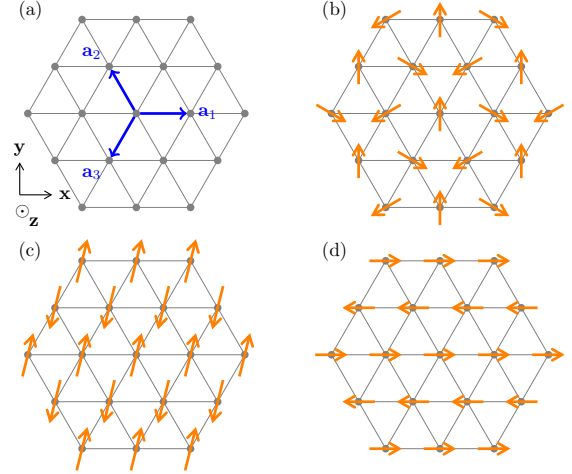


FIG. 1. (a) Yb^{3+} ions in YbMgGaO_4 form a perfect triangular lattice. The inset defines the coordinate system for the spin components. (b) The 120° state in region I. (c) The stripe order in region II with spins pointing in the yz plane. (d) The stripe order in region III with spins pointing along the x direction.

field. The lowest Kramers' doublet is well separated from the upper excited doublets by a large crystal electric field gap ($\Delta \sim 420\text{K}$) [6]. In the low temperature regime ($T \ll \Delta$), only the ground state Kramers' doublet is active, and we introduce an effective spin-1/2 local moment \mathbf{S}_i that operates on the local ground state Kramers' doublet. Because of the spin-orbit entangled nature of the local moment and the predominant contribution from the orbital part, the interaction between the effective spin-1/2 moments is *anisotropic* both in the effective spin space and in the position space [8–15]. The most generic

spin Hamiltonian allowed by the space group symmetry of YbMgGaO_4 is given by [6, 16]

$$\begin{aligned} \mathcal{H} = & \sum_{\langle ij \rangle} J_{zz} S_i^z S_j^z + J_{\pm} (S_i^+ S_j^- + S_i^- S_j^+) \\ & + J_{\pm\pm} (\gamma_{ij} S_i^+ S_j^+ + \gamma_{ij}^* S_i^- S_j^-) \\ & - \frac{iJ_{z\pm}}{2} (\gamma_{ij}^* S_i^+ S_j^z - \gamma_{ij} S_i^- S_j^z + \langle i \leftrightarrow j \rangle), \quad (1) \end{aligned}$$

where $S_i^{\pm} = S_i^x \pm iS_i^y$, and $\gamma_{ij} = 1, e^{i2\pi/3}, e^{-i2\pi/3}$ for the bond ij along the $\mathbf{a}_1, \mathbf{a}_2, \mathbf{a}_3$ directions, respectively (see Fig. 2a). This generic model can be generally applied to any other Kramers' doublet on the triangular lattice, so its application is *beyond* the Yb^{3+} local moment of YbMgGaO_4 .

In this paper we carry out the semiclassical analysis of the generic spin Hamiltonian. We first determine the classical ground state phase diagram of the model and find three different ordered phases by the Luttinger-Tisza method. Then we implement the classical Monte Carlo simulation to uncover the classical magnetic orders at low temperatures. The ordering temperatures of different phases are determined as well. We find that the ordering temperatures obtained from classical Monte Carlo are strongly suppressed near the the phase boundary between different phases, suggesting the strong frustration in these regions. We further study the quantum fluctuation through a self-consistent spin wave theory and find that the quantum fluctuation is very strong and could melt the magnetic order in the parameter regimes near the phase boundary. We thus expect these regions may turn into the QSLs when the quantum nature of the spins is considered.

Luttinger-Tisza method.—We treat the spin as a classical vector that satisfies the constraint $|\mathbf{S}_i| = 1/2$. Following Luttinger and Tisza [17], we first replace the hard spin constraint with a global constraint such that $\sum_i |\mathbf{S}_i|^2 = N/4$ where N is the total number of spins. The classical spin Hamiltonian is then minimized under this global constraint. If the energy minimum turns out to satisfy the local constraint as well, then this energy minimum is the true classical ground state.

When $J_{\pm\pm} = 0$ and $J_{z\pm} = 0$, the spin model reduces to the XXZ model. From the experimental results on single crystal samples [6], one finds that both J_{zz} and J_{\pm} are antiferromagnetic and $J_{\pm}/J_{zz} \approx 0.915$ which is fixed to this value throughout the paper. The ground state of this XXZ model is simply the well-known 120° ordered state with the spins orienting in the xy plane (see Fig. 2b). The ordering wavevector of the 120° state is at $\mathbf{k}_c = (4\pi/3, 0)$ or its symmetry equivalent wavevectors.

With a small $|J_{\pm\pm}|$, the minimum of the classical Hamiltonian under the global constraint slightly deviates from the 120° state and occurs at incommensurate wavevectors. In strong spin-orbit coupled insulators, however, the incommensurate ordering is generically not

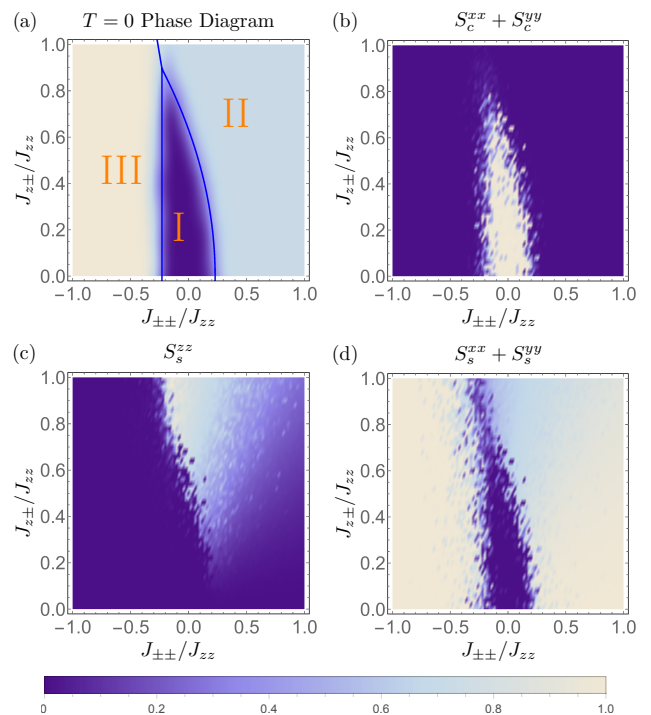


FIG. 2. (a) The classical phase diagram in the zero temperature limit (see the text for discussion). The (blue) solid lines are the phase boundaries that are obtained by the Luttinger-Tisza method, and the (colored) phase regions are obtained by classical Monte Carlo simulation. In (b), (c) and (d), spin-spin correlation functions $S_{c/s}^{\alpha\beta}$ at zero temperature are displayed. (b) $S_c^{xx} + S_c^{yy}$ at $T \rightarrow 0$. The region with large S_c suggests the 120° order of spins. (c) A finite z - z correlation for the stripe phase helps us distinguish two stripe phases (Fig. 2c and d) due to different signs of $J_{\pm\pm}$. (d) x - x plus y - y correlation for the stripe phase.

avored. Because of the intrinsic spin anisotropy that originates from the strong spin-orbit coupling [18], if the ordered spin moments orient freely like the case for an incommensurate state, the spin anisotropy would not be optimized. As a result, we generically have the commensurate spin orders in the strong spin-orbit coupled insulators. Apart from the generic argument, we here provide more specific reasons. Due to the low symmetry of the Hamiltonian, the eigenstate that corresponds to the minimum is generically unique, hence one cannot find two orthogonal eigenvectors to construct an incommensurate spiral state that satisfies the hard spin constraint on every lattice site. Therefore, the incommensurate state cannot be a true classical ground state, and we tentatively regard the 120° state as the candidate classical ground state in the regime with a small $J_{\pm\pm}$.

With a large $|J_{\pm\pm}|$ and/or a large $|J_{z\pm}|$, the minimum of the classical Hamiltonian occurs at $\mathbf{k}_s = (0, 2\pi/\sqrt{3})$ or its symmetry equivalent wavevectors. Remarkably, this minimum state satisfies the hard spin constraint and is thus a true ground state. The spin configuration with

this ordering wavevector has a stripe order, *i.e.*, the spins order ferromagnetically along one lattice direction and antiferromagnetically along the remaining two lattice directions. To obtain the classical phase diagram in Fig. 2a, we compare the energies of the 120° state and the stripe ordered phases. In the region I of the phase diagram, the 120° state is obtained. In the region II and III, we find two stripe ordered phases with different spin orientations. Without loss of generality, we fix the ordering wavevector of the stripe phase to be $\mathbf{k}_s = (0, 2\pi/\sqrt{3})$. Due to the locking of the spin orientation and the ordering wavevector, the spin configuration is fixed as well. With this choice of the ordering wavevector, the spins are pointing in the yz plane [19] and x direction in region II and region III, respectively (see Fig. 2).

Here we elucidate the structure of the phase diagram. The magnetic phases for a negative $J_{z\pm}$ can be simply generated from the ones in the positive $J_{z\pm}$ case by a 180° rotation around the z axis. Under this rotation ($S_i^z \rightarrow S_i^z$ and $S_i^\pm \rightarrow -S_i^\pm$), the coupling $J_{z\pm} \rightarrow -J_{z\pm}$ while other couplings stay invariant [20]. Therefore, we only consider the phase diagram with a positive $J_{z\pm}$ in Fig. 2. In addition, on the horizontal axis with $J_{z\pm} = 0$, the magnetic phases are symmetric about the origin. This is seen by rotating the spins around the z axis by 90° . It transforms the spins as $S_i^z \rightarrow S_i^z$, $S_i^\pm \rightarrow \pm i S_i^\pm$ and the coupling as $J_{\pm\pm} \rightarrow -J_{\pm\pm}$. The above properties of the phase diagram hold even in the quantum regime.

Classical Monte Carlo.—To further investigate the structure of the classical phase diagram and to extract finite-temperature magnetic properties, we implement the classical Monte Carlo simulation of the classical spin Hamiltonian [21, 22]. As we previously explained, the system prefers the commensurate spin orders. So one does not need a large system size to carry out the classical Monte Carlo simulation. The simulation is performed on 6×6 and 12×12 triangular systems. It starts with a randomly chosen initial spin configuration, followed by 5000 transient Monte Carlo steps (MCS) for the system to equilibrate. Within each step, the Metropolis algorithm [23, 24] is implemented for sampling, and a method proposed in [25] is used for updating the spin configurations in the canonical ensemble. The observables are averaged within a sample of size MCS = 50000.

Since the 120° state (the stripe ordered phase) has an ordering wavevector \mathbf{k}_c (\mathbf{k}_s), we evaluate the spin-spin correlation functions at the corresponding wavevectors,

$$S_{c/s}^{\alpha\beta} = \frac{1}{N^2} \sum_{i,j} \langle S_i^\alpha S_j^\beta \rangle e^{i\mathbf{k}_{c/s} \cdot (\mathbf{r}_j - \mathbf{r}_i)}, \quad (2)$$

where $\alpha, \beta = x, y, z$. The result is summarized in Fig. 2. In the zero temperature limit, we observe a significant stripe order that signifies the stripe phases away from the central region of the phase diagram. We also notice that as both $J_{\pm\pm}$ and $J_{z\pm}$ increase on the positive side,

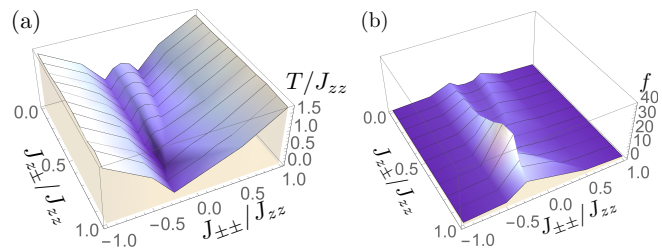


FIG. 3. (a) Finite temperature phase diagram. The lines are constant $J_{z\pm}/J_{zz}$ cuts, which are given in the supplementary material [16]. The surface represents the critical temperature for different values of $J_{z\pm}$ and $J_{\pm\pm}$. Above this surface the system is in the paramagnetic phase. The region beneath the central dome-like surface corresponds to the 120° phase. The other regions under the surface are stripe-ordered, corresponding to regions II and III in Fig. 2a at zero temperature. (b) The frustration parameter $f \equiv |\Theta_{CW}|/T_c$.

the spins develop a finite component in the yz plane, distinguishing it from the stripe order with spins pointing along x direction in the negative $J_{\pm\pm}$ region (region II in Fig. 2a).

Near the phase boundaries, not only the neighboring ordered phases are very close in energies, but a large number of classical spin configurations have rather close energies. As a result, thermal fluctuations can easily populate the low energy spin configurations even at a temperature much smaller than $|\Theta_{CW}|$ such that the system may not favor any obvious magnetic order. Therefore, we expect the ordering temperature to be strongly suppressed in these frustrated regions.

The classical Monte Carlo simulation allows us to access the finite temperature magnetic properties. We can still perform the calculation of the spin correlation function as the temperature is raised from zero. At zero temperature, the system is frozen at its ground state, therefore the deviation of a physical observable \hat{O} (chosen to be $S^{\alpha\beta}$ in this case), $\langle \hat{O}^2 \rangle - \langle \hat{O} \rangle^2$, vanishes. However, at finite temperatures, due to the possibility for spins to flip to another configuration with similar energy, \hat{O} can develop a nonzero deviation. Therefore, the Binder ratios [26, 27], defined for the spin-spin correlation functions,

$$r^{\alpha\alpha} = \frac{\langle (S_{c/s}^{\alpha\alpha})^2 \rangle}{\langle S_{c/s}^{\alpha\alpha} \rangle^2}, \quad (3)$$

should attain the value 1 at zero temperature, and saturate to a larger value in the high temperature limit. The Binder ratios are scale-independent quantities at the critical temperature T_c , hence T_c can be estimated by finding the crossing of $r^{\alpha\alpha} - T$ curves for different lattice sizes. The thermal transition is found to be continuous and no other thermal phases are found in our numerical study of finite size systems. The result of our simulation is summarized in Fig. 3a.

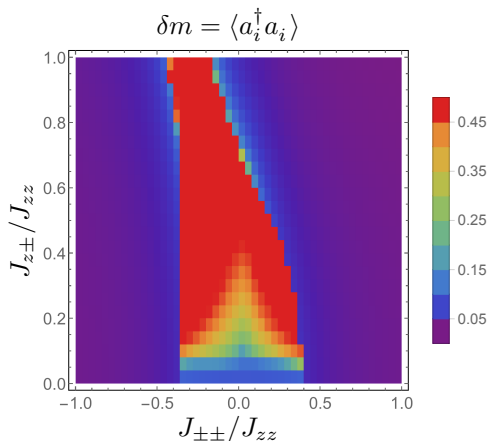


FIG. 4. Quantum correction (δm) to the magnetic orders that is calculated within the self-consistent spin wave theory on a 80×80 lattice [16]. The region near phase boundary where δm exceeds the spin magnitude with $\delta m \geq 1/2$ is marked in red.

It is found that in the parameter regimes near the phase boundary the magnetic ordering temperature is in fact strongly suppressed compared to the Curie-Weiss temperature $|\Theta_{\text{CW}}|$. The local moments do not order down to very low temperatures, which indicates the strong spin frustration in these regions. In Fig. 3b, we evaluate the frustration parameter ($f \equiv |\Theta_{\text{CW}}|/T_c$) that is an empirical measure of the frustration [28]. Because of the spin anisotropy, the Curie-Weiss temperature depends on the direction of the external magnetic field. To be specific, we choose the Curie-Weiss temperature to be the one when the external field is applied in the xy plane, so we have $\Theta_{\text{CW}} = -3J_{\pm}$ [6]. Indeed, the frustration parameter is as large as 20 near the phase boundaries between two neighboring phases (Fig. 3b) [16].

Self-consistent spin-wave theory.—Here we go beyond the classical treatment and consider the quantum fluctuation to the magnetic orders. Deep inside each ordered phase, the magnetic order is robust, and we expect that the quantum fluctuation only slightly renormalizes the magnetic order. In contrast, near the phase boundary, many classical states have rather close energies and would enhance the quantum fluctuations. To demonstrate this explicitly, we apply the Dyson-Maleev transformation for the spin operators and solve for the quantum correction to the magnetic order within a self-consistent spin wave theory [16, 29, 30]. As we show in Fig. 3, the quantum fluctuation is indeed quite strong and melts the magnetic order in the region near the phase boundary.

Discussions.—Although our treatment of the generic spin model is mostly semiclassical and the ground states that we found are magnetically ordered, our results are quite suggestive for identifying the parameter regime of possible QSL ground state of the generic model for the

quantum spins. We have showed that the quantum fluctuation is indeed quite strong in certain parameter regime and could in fact completely destroy the magnetic order itself. Therefore, if the QSL ground state appears in the phase diagram of the generic spin model for the triangular lattice, it would most likely occur in these frustrated regions near the phase boundaries between different ordered states. Our current study thus provides a useful guidance and is a benchmark for the future numerical study of this generic spin model.

To summarize, we analyzed the generic spin Hamiltonian that describes the interaction between the spin-orbit-entangled Kramers' doublet local moments. We have obtained the full classical phase diagram and identified the frustrated region that might host the QSL ground state for the Yb local moments in YbMgGaO_4 . As the generic model applies to any other Kramers' doublet with the same symmetry properties as the Yb one, to further justify the applicability of this model, it is thus of great interest to experimentally study the magnetic properties of other rare-earth based triangular materials and access the magnetic ground states and the magnetic transition from the possible QSL state. Apart from the rare-earth systems, the spin-orbit-entangled Kramers' doublet local moments can appear in the partially filled t_{2g} shells [8, 31]. Given the 4d or 5d nature of the local moments, the exchange interaction is certainly enhanced, and thus one could probe the magnetic and the QSL physics at a much higher temperature than the rare-earth systems.

Acknowledgements.—We acknowledge Yuesheng Li (Renmin Univ), Xiaoqun Wang (Renmin Univ), and Qingming Zhang (Renmin Univ) for the previous collaboration, Leon Balents and Patrick Lee for correspondences. We thank Xi Dai, Fengren Fan, Jiangping Hu, Dunghai Lee, Shiyao Li, Yuanming Lu, Yang Qi, Fa Wang, Nanlin Wang, Zhong Wang, Hua Wu, Hong Yao, Rong Yu, Yue Yu, Jize Zhao, Fuchun Zhang, Jun Zhao, and Yi Zhou for valuable conversation. We are particularly indebted to Zhong Wang at Institute of Advanced Study of Tsinghua University for hosting our stay where part of the work was completed.

* chggst@gmail.com, or, gchen_physics@fudan.edu.cn

- [1] Patrick A. Lee, "An end to the drought of quantum spin liquids," *Science* **321**, 1306–1307 (2008).
- [2] Leon Balents, "Spin liquids in frustrated magnets," *Nature* **464**, 199–208 (2010).
- [3] Alexei Kitaev, "Anyons in an exactly solved model and beyond," *Annals of Physics* **321**, 2 – 111 (2006), January Special Issue.
- [4] X.-G. Wen, *Quantum Field Theory of Many-body Systems: From the Origin of Sound to an Origin of Light and Electrons*, reissue ed. (Oxford University Press, New

- York, USA, 2007).
- [5] H. Watanabe, H. C. Po, A. Vishwanath, and M. P. Zaletel, “Lieb-schultz-mattis theorems in the presence of spin-orbit coupling: filling constraints for insulators in symmorphic and non-symmorphic crystals,” arXiv:1505.04193 (2015).
- [6] Yuesheng Li, Gang Chen, Wei Tong, Li Pi, Juanjuan Liu, Zhaorong Yang, Xiaoqun Wang, and Qingming Zhang, “Rare-earth triangular lattice spin liquid: A single-crystal study of ybmggao_4 ,” *Phys. Rev. Lett.* **115**, 167203 (2015).
- [7] Yuesheng Li, Haijun Liao, Zhen Zhang, Shiyang Li, Feng Jin, Langsheng Ling, Lei Zhang, Youming Zou, Li Pi, Zhaorong Yang, Junfeng Wang, Zhonghua Wu, and Qingming Zhang, “Gapless quantum spin liquid ground state in the two-dimensional spin-1/2 triangular antiferromagnet ybmggao_4 ,” *Scientific Reports* **5**, 16419 (2015).
- [8] Gang Chen and Leon Balents, “Spin-orbit effects in $\text{na}_4\text{ir}_3\text{os}_8$: A hyper-kagome lattice antiferromagnet,” *Phys. Rev. B* **78**, 094403 (2008).
- [9] William Witczak-Krempa, Gang Chen, Yong Baek Kim, and Leon Balents, “Correlated quantum phenomena in the strong spin-orbit regime,” *Annual Review of Condensed Matter Physics* **5**, 57–82 (2014).
- [10] Kai Li, Shun-Li Yu, and Jian-Xin Li, “Global phase diagram, possible chiral spin liquid, and topological superconductivity in the triangular kitaevheisenberg model,” *New Journal of Physics* **17**, 043032 (2015).
- [11] Gang Chen, Rodrigo Pereira, and Leon Balents, “Exotic phases induced by strong spin-orbit coupling in ordered double perovskites,” *Phys. Rev. B* **82**, 174440 (2010).
- [12] S. H. Curnoe, “Structural distortion and the spin liquid state in $\text{tb}_2\text{ti}_2\text{o}_7$,” *Phys. Rev. B* **78**, 094418 (2008).
- [13] Shigeki Onoda and Yoichi Tanaka, “Quantum melting of spin ice: Emergent cooperative quadrupole and chirality,” *Phys. Rev. Lett.* **105**, 047201 (2010).
- [14] Gang Chen and Leon Balents, “Spin-orbit coupling in d^2 ordered double perovskites,” *Phys. Rev. B* **84**, 094420 (2011).
- [15] G. Jackeli and G. Khaliullin, “Mott insulators in the strong spin-orbit coupling limit: From heisenberg to a quantum compass and kitaev models,” *Phys. Rev. Lett.* **102**, 017205 (2009).
- [16] See the supplementary material for the detailed information.
- [17] J. M. Luttinger and L. Tisza, “Theory of dipole interaction in crystals,” *Phys. Rev.* **70**, 954–964 (1946).
- [18] Hiroaki Ishizuka and Leon Balents, “Switching of magnetic anisotropy in a fcc antiferromagnet with direction-dependent interactions,” *Phys. Rev. B* **92**, 020411 (2015).
- [19] The actual spin orientation depends on the couplings.
- [20] Lucile Savary and Leon Balents, “Coulombic quantum liquids in spin-1/2 pyrochlores,” *Phys. Rev. Lett.* **108**, 037202 (2012).
- [21] Hikaru Kawamura and Seiji Miyashita, “Phase transition of the two-dimensional heisenberg antiferromagnet on the triangular lattice,” *Journal of the Physical Society of Japan* **53**, 4138–4154 (1984).
- [22] B.W. Southern and H-J. Xu, “Monte carlo study of the heisenberg antiferromagnet on the triangular lattice,” *Phys. Rev. B* **52**, R3836–R3839 (1995).
- [23] Nicholas Metropolis, Arianna W. Rosenbluth, Marshall N. Rosenbluth, Augusta H. Teller, and Edward Teller, “Equation of state calculations by fast computing machines,” *The Journal of Chemical Physics* **21**, 1087–1092 (1953).
- [24] W. K. Hastings, “Monte carlo sampling methods using markov chains and their applications,” *Biometrika* **57**, 97–109 (1970).
- [25] George Marsaglia, “Choosing a point from the surface of a sphere,” *Ann. Math. Statist.* **43**, 645–646 (1972).
- [26] K. Binder, “Finite size scaling analysis of ising model block distribution functions,” *Zeitschrift für Physik B Condensed Matter* **43**, 119–140 (1981).
- [27] K Binder, “Applications of monte carlo methods to statistical physics,” *Reports on Progress in Physics* **60**, 487 (1997).
- [28] A P Ramirez, “Strongly geometrically frustrated magnets,” *Annual Review of Materials Science* **24**, 453–480 (1994).
- [29] Freeman J. Dyson, “General theory of spin-wave interactions,” *Phys. Rev.* **102**, 1217–1230 (1956).
- [30] S. V. Maleev, *Sov. Phys. JETP* **64**, 654 (1958).
- [31] B. J. Kim, H. Ohsumi, T. Komesu, S. Sakai, T. Morita, H. Takagi, and T. Arima, “Phase-sensitive observation of a spin-orbital mott state in sr_2iro_4 ,” *Science* **323**, 1329–1332 (2009).
- [32] Kate A. Ross, Lucile Savary, Bruce D. Gaulin, and Leon Balents, “Quantum excitations in quantum spin ice,” *Phys. Rev. X* **1**, 021002 (2011).
- [33] C. M. Canali, S. M. Girvin, and Mats Wallin, “Spin-wave velocity renormalization in the two-dimensional heisenberg antiferromagnet at zero temperature,” *Phys. Rev. B* **45**, 10131–10134 (1992).
- [34] Adrian Del Maestro and Michel J. P. Gingras, “Low-temperature specific heat and possible gap to magnetic excitations in the heisenberg pyrochlore antiferromagnet $\text{gd}_2\text{sn}_2\text{o}_7$,” *Phys. Rev. B* **76**, 064418 (2007).

SUPPLEMENTARY INFORMATION FOR “A SEMICLASSICAL STUDY OF THE GENERIC SPIN MODEL ON A TRIANGULAR LATTICE”

Space group symmetry and the generic spin model for YbMgGaO_4

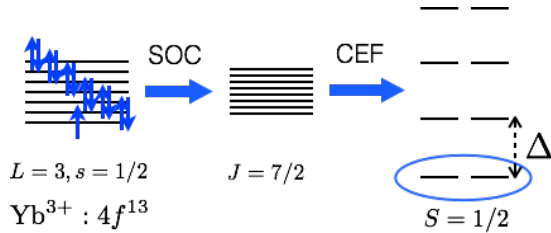


FIG. 1. The formation of the local ground state Kramers’ doublet under the combination of spin-orbit coupling (SOC) and the crystal electric field (CEF). Please refer the text for the detailed description.

The Yb^{3+} ion contains thirteen $4f$ electrons. According to the Hund’s rule, we should have the total spin $s = 1/2$ and the orbital angular momentum $L = 3$ for the Yb^{3+} ion. The fourteen-fold spin and orbital degeneracy should be lifted when the atomic spin-orbit coupling and the crystal electric field are considered. For the $4f$ electrons, the atomic spin-orbit coupling should be considered before the crystal electric field. As we show in Fig. 2, the atomic spin-orbit coupling entangles the orbital angular momentum and the total spin, leading to a total angular momentum $J = 7/2$. Just like the case for the quantum spin ice candidate $\text{Yb}_2\text{Ti}_2\text{O}_7$ [32], the crystal electric field of the D_{3d} point group further splits the eight $J = 7/2$ states into four pairs of Kramers’ doublets. The ground state doublet is well separated from other excited doublets with an energy gap Δ and thus can be treated as an effective spin-1/2 degree of freedom at the temperature that is much lower than the energy gap [7, 32]. This effective spin-1/2 degree of freedom for the Yb^{3+} ion is further supported by the low temperature magnetic entropy that is measured to be $R \ln 2$ per spin [6, 7].

This effective spin, denoted as \mathbf{S} in the main text, results from the spin-orbital entanglement of the Yb^{3+} $4f$ electrons. As a consequence, under the space group symmetry operation, both the position and the orientation of the spins are transformed as

$$\mathbf{S}_{\mathbf{r}} \rightarrow \text{Det}[\hat{O}] \cdot \hat{O}^{-1} \cdot \mathbf{S}_{\hat{O} \cdot \mathbf{r} + \mathbf{t}}, \quad (1)$$

where \hat{O} and \mathbf{t} are the matrix and the vector that specify the rotation part and the translation part of the space group operation, respectively. In contrast, in a magnetic system whose local moment is purely given by the total spin, the spin rotational symmetry would be decoupled from the space group symmetry operation. The latter

merely acts on the positions of the spin moments and does not rotate the spin components. This is the key difference between the strong spin-orbit coupled Mott insulators and a conventional Mott insulator with quenched orbital degrees of freedom.

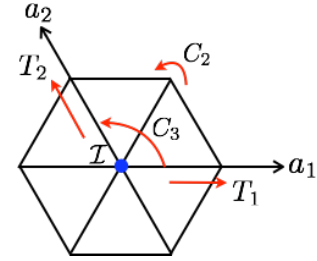


FIG. 2. The space group symmetry operation for the Yb triangular layer.

As we explain in the main text, the interlayer Yb spin coupling is much weaker than the intralayer one. We thus keep the symmetry operation within each Yb triangular layer. The $R\bar{3}m$ space group symmetry contains two translations (T_1 and T_2) along the two crystallographic axes, the three-fold rotation (C_3) around the z direction, the two-fold rotation (C_2) around the diagonal direction, and an inversion (\mathcal{I}) about the lattice site. With these symmetries and their transformations on the spin operators, it is ready to obtain the generic spin Hamiltonian that describes the interaction between the Yb local moments,

$$\begin{aligned} \mathcal{H} = & \sum_{\langle ij \rangle} J_{zz} S_i^z S_j^z + J_{\pm} (S_i^+ S_j^- + S_i^- S_j^+) \\ & + J_{\pm\pm} (\gamma_{ij} S_i^+ S_j^+ + \gamma_{ij}^* S_i^- S_j^-) \\ & - \frac{iJ_{z\pm}}{2} (\gamma_{ij}^* S_i^+ S_j^z - \gamma_{ij} S_i^- S_j^z + \langle i \leftrightarrow j \rangle). \quad (2) \end{aligned}$$

Frustration parameters

In Fig. 3 and Fig. 4, we disassemble the three-dimensional plots of the transition temperature and the frustration parameter into a set of two-dimensional plots.

Self-consistent spin wave theory

In this section, we provide a detailed derivation of the spin wave theory. We focus the discussion on the stripe ordered phase in region III, and the spin wave theory in other ordered regions can be obtained likewise. As we show in the main text, the spins in region III orient in the $\pm \hat{x}$ directions. We introduce the Dyson-Maleev representation for the spin operators [29, 30]

$$\mathbf{S}_i \cdot \hat{m}_i = -S + a_i^\dagger a_i, \quad (3)$$

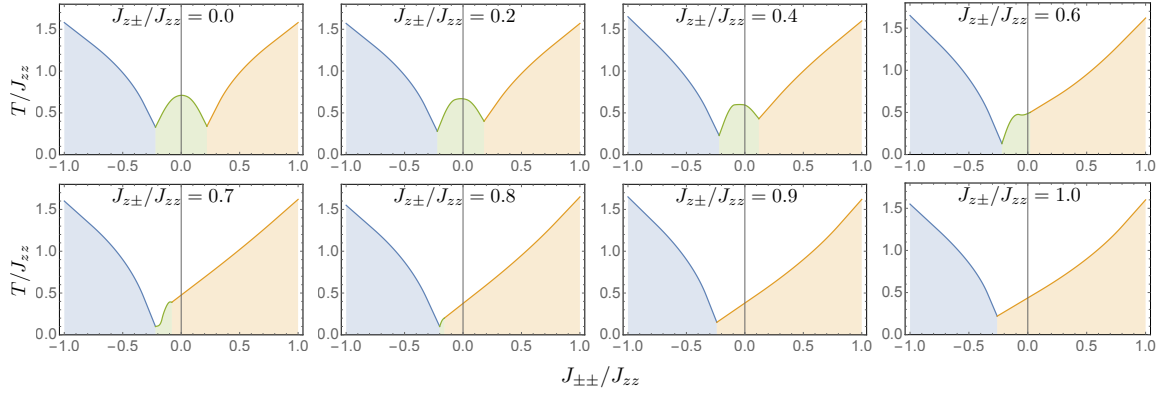


FIG. 3. Cuts through constant $J_{z\pm}$ lines of through the three-dimensional finite temperature phase diagram in the main text. The white region is the high temperature paramagnetic phase. The solid line indicates the transition temperatures.

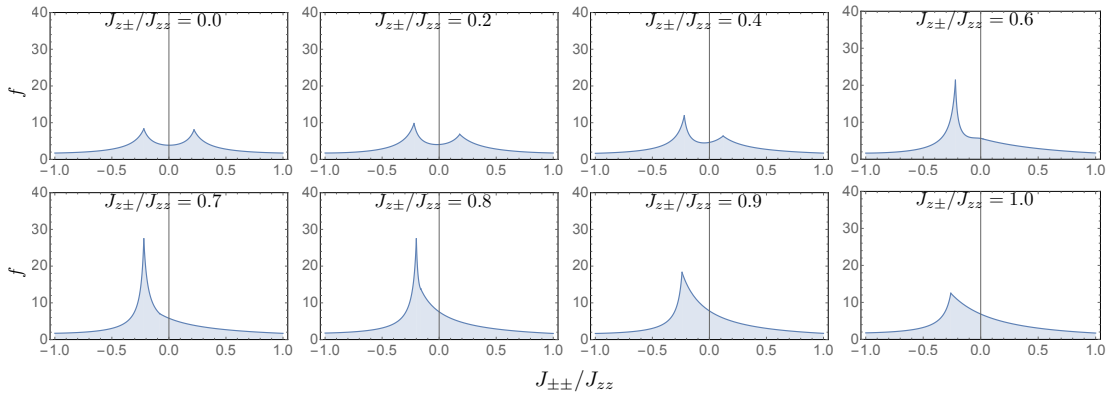


FIG. 4. The frustration parameter $f \equiv |\Theta_{CW}|/T_N$ of the corresponding plots in Fig. 3.

$$\mathbf{S}_i \cdot \hat{z} = \frac{1}{2}[a_i^\dagger(2S - a_i^\dagger a_i) + a_i], \quad (4)$$

$$\mathbf{S}_i \cdot [\hat{m}_i \times \hat{z}] = \frac{1}{2i}[a_i^\dagger(2S - a_i^\dagger a_i) - a_i], \quad (5)$$

where $S = 1/2$, \hat{m}_i is the direction of the classical spin order and points along \hat{x} or $-\hat{x}$. Because the classical ground state has two sublattices, there will be two flavors of Dyson-Maleev bosons that describe the magnetic excitation and quantum fluctuation of region III.

In the usual linear spin wave approximation, one first neglects the cubic boson terms in the Dyson-Maleev transformation by setting

$$\mathbf{S}_i \cdot \hat{m}_i = -S + a_i^\dagger a_i, \quad (6)$$

$$\mathbf{S}_i \cdot \hat{z} \approx (a_i^\dagger + a_i)/2 \quad (7)$$

$$\mathbf{S}_i \cdot [\hat{m}_i \times \hat{z}] \approx (a_i^\dagger - a_i)/(2i). \quad (8)$$

This approximation is valid when $\langle a_i^\dagger a_i \rangle \ll S$. We substitute the spin operators with the Dyson-Maleev bosons, keep the quadratic part of the spin-wave Hamiltonian,

and diagonalize it with the standard Bogoliubov transformation. We proceed to evaluate the quantum correction $\delta m_i \equiv \langle a_i^\dagger a_i \rangle$ and find that δm_i is quite large in the parameter regime near the phase boundary. Clearly, the strong quantum fluctuation in these regions invalidates the assumption of the linear spin-wave theory that neglects the spin wave interaction.

To fix the drawbacks of the linear spin-wave approximation, we implement a self-consistent spin-wave calculation in the following. The Dyson-Maleev transformation in Eqs. (3)-(5) has proven to be convenient for studying spin-wave interaction [33]. With the Dyson-Maleev transformation for the spin operators, we obtain the spin wave Hamiltonian. In the spin-wave Hamiltonian, there exist cubic, quartic, quintic, and sextic terms in the Dyson-Maleev bosons. To reduce the spin wave Hamiltonian down to the quadratic level, we first make the approximation by keeping the boson terms up to the sextic order, and then make the mean-field decoupling of the quartic and sextic terms. The quartic and sextic terms are decoupled into various on-site and intersite boson bilinears,

$$\begin{aligned}
a_i^\dagger a_i a_j^\dagger a_j &\rightarrow [a_i^\dagger a_i - \langle a_i^\dagger a_i \rangle] \langle a_j^\dagger a_j \rangle + \langle a_i^\dagger a_i \rangle [a_j^\dagger a_j - \langle a_j^\dagger a_j \rangle] \\
&\quad + \langle a_i^\dagger a_j^\dagger \rangle [a_i a_j - \langle a_i a_j \rangle] + [a_i^\dagger a_j^\dagger - \langle a_i^\dagger a_j^\dagger \rangle] \langle a_i a_j \rangle \\
&\quad + \langle a_i^\dagger a_j \rangle [a_j^\dagger a_i - \langle a_j^\dagger a_i \rangle] + [a_i^\dagger a_j - \langle a_i^\dagger a_j \rangle] \langle a_j^\dagger a_i \rangle \\
&\quad + \langle a_i^\dagger a_i \rangle \langle a_j^\dagger a_j \rangle + \langle a_i^\dagger a_j^\dagger \rangle \langle a_i a_j \rangle + \langle a_i^\dagger a_j \rangle \langle a_j^\dagger a_i \rangle,
\end{aligned} \tag{9}$$

$$\begin{aligned}
a_i^\dagger a_j^\dagger a_j^\dagger a_j &\rightarrow [a_j^\dagger a_j^\dagger - \langle a_j^\dagger a_j^\dagger \rangle] \langle a_i^\dagger a_j \rangle + a_j^\dagger a_j^\dagger [a_i^\dagger a_j - \langle a_i^\dagger a_j \rangle] \\
&\quad + 2[a_j^\dagger a_j - \langle a_j^\dagger a_j \rangle] \langle a_i^\dagger a_j^\dagger \rangle + 2\langle a_j^\dagger a_j \rangle [a_i^\dagger a_j^\dagger - \langle a_i^\dagger a_j^\dagger \rangle] \\
&\quad + \langle a_j^\dagger a_j^\dagger \rangle \langle a_i^\dagger a_j \rangle + 2\langle a_j^\dagger a_j \rangle \langle a_i^\dagger a_j^\dagger \rangle,
\end{aligned} \tag{10}$$

$$\begin{aligned}
a_i^\dagger a_i^\dagger a_i a_j^\dagger a_j^\dagger a_j &\rightarrow [a_i^\dagger a_i^\dagger - \langle a_i^\dagger a_i^\dagger \rangle] \langle a_i a_j^\dagger a_j^\dagger a_j \rangle + 2[a_i^\dagger a_i - \langle a_i^\dagger a_i \rangle] \langle a_i^\dagger a_j^\dagger a_j^\dagger a_j \rangle \\
&\quad + [a_j^\dagger a_j^\dagger - \langle a_j^\dagger a_j^\dagger \rangle] \langle a_i^\dagger a_i^\dagger a_i a_j \rangle + 2[a_j^\dagger a_j - \langle a_j^\dagger a_j \rangle] \langle a_i^\dagger a_i^\dagger a_i a_j^\dagger \rangle \\
&\quad + 4[a_i^\dagger a_j^\dagger - \langle a_i^\dagger a_j^\dagger \rangle] \langle a_i^\dagger a_i a_j^\dagger a_j \rangle + 2[a_i^\dagger a_j - \langle a_i^\dagger a_j \rangle] \langle a_i^\dagger a_i a_j^\dagger a_j^\dagger \rangle \\
&\quad + 2[a_i a_j^\dagger - \langle a_i a_j^\dagger \rangle] \langle a_i^\dagger a_i^\dagger a_j^\dagger a_j \rangle + [a_i a_j - \langle a_i a_j \rangle] \langle a_i^\dagger a_i^\dagger a_j^\dagger a_j^\dagger \rangle \\
&\quad + \langle a_i^\dagger a_i^\dagger a_i a_j^\dagger a_j^\dagger a_j \rangle,
\end{aligned} \tag{11}$$

where the expectation “ $\langle \dots \rangle$ ” is evaluated with respect to the ground state of the quadratic spin wave Hamiltonian that is defined later. We have

$$\begin{aligned}
\langle a_i^\dagger a_i^\dagger a_i a_j^\dagger a_j^\dagger a_j \rangle &= 2\langle a_i^\dagger a_i^\dagger \rangle \langle a_i a_j^\dagger \rangle \langle a_j^\dagger a_j \rangle + \langle a_i^\dagger a_i^\dagger \rangle \langle a_j^\dagger a_j^\dagger \rangle \langle a_i a_j \rangle + 4\langle a_i^\dagger a_i \rangle \langle a_j^\dagger a_j \rangle \langle a_i^\dagger a_j^\dagger \rangle \\
&\quad + 2\langle a_i^\dagger a_i \rangle \langle a_j^\dagger a_j^\dagger \rangle \langle a_i^\dagger a_j \rangle + 4\langle a_i^\dagger a_j^\dagger \rangle \langle a_i^\dagger a_j \rangle \langle a_i a_j^\dagger \rangle + 2\langle a_i^\dagger a_j^\dagger \rangle \langle a_i^\dagger a_j^\dagger \rangle \langle a_i a_j \rangle,
\end{aligned} \tag{12}$$

and

$$\langle a_i a_j^\dagger a_j^\dagger a_j \rangle = 2\langle a_i a_j^\dagger \rangle \langle a_j^\dagger a_j \rangle + \langle a_i a_j \rangle \langle a_j^\dagger a_j^\dagger \rangle, \tag{13}$$

$$\langle a_i^\dagger a_j^\dagger a_j^\dagger a_j \rangle = 2\langle a_i^\dagger a_j^\dagger \rangle \langle a_j^\dagger a_j \rangle + \langle a_i^\dagger a_j \rangle \langle a_j^\dagger a_j^\dagger \rangle, \tag{14}$$

$$\langle a_i^\dagger a_i^\dagger a_i a_j \rangle = 2\langle a_i^\dagger a_i^\dagger \rangle \langle a_i a_j \rangle + \langle a_i^\dagger a_i \rangle \langle a_i a_j^\dagger \rangle, \tag{15}$$

$$\langle a_i^\dagger a_i^\dagger a_i a_j^\dagger \rangle = 2\langle a_i^\dagger a_i^\dagger \rangle \langle a_i a_j^\dagger \rangle + \langle a_i^\dagger a_i \rangle \langle a_i a_j \rangle, \tag{16}$$

$$\begin{aligned}
\langle a_i^\dagger a_i a_j^\dagger a_j \rangle &= \langle a_i^\dagger a_i \rangle \langle a_j^\dagger a_j \rangle + \langle a_i^\dagger a_j^\dagger \rangle \langle a_i a_j \rangle \\
&\quad + \langle a_i^\dagger a_j \rangle \langle a_j^\dagger a_i \rangle,
\end{aligned} \tag{17}$$

$$\langle a_i^\dagger a_i a_i^\dagger a_j^\dagger \rangle = \langle a_i^\dagger a_i \rangle \langle a_j^\dagger a_j^\dagger \rangle + 2\langle a_i^\dagger a_j^\dagger \rangle \langle a_i a_j^\dagger \rangle, \tag{18}$$

$$\langle a_i^\dagger a_i^\dagger a_j^\dagger a_j \rangle = 2\langle a_i^\dagger a_j^\dagger \rangle \langle a_i^\dagger a_j \rangle + \langle a_i^\dagger a_i \rangle \langle a_j^\dagger a_j \rangle, \tag{19}$$

$$\langle a_i^\dagger a_i^\dagger a_j^\dagger a_j^\dagger \rangle = 2\langle a_i^\dagger a_j^\dagger \rangle \langle a_i^\dagger a_j^\dagger \rangle + \langle a_i^\dagger a_i \rangle \langle a_j^\dagger a_j^\dagger \rangle. \tag{20}$$

The decoupling of the cubic and quintic terms leads to linear terms in the Dyson-Maleev bosons that should all cancel out by the stability requirement of the classical ground state. Therefore, the decoupling of the cubic and quintic terms does not introduce extra quadratic terms into the spin-wave Hamiltonian.

After defining the Fourier transform of the Dyson-Maleev boson operators, the quadratic spin-wave Hamiltonian can be organized as

$$H_{\text{sw}} = \sum_{\mathbf{k}} (A_{\mathbf{k}}^\dagger, A_{-\mathbf{k}}) \begin{pmatrix} F_{\mathbf{k}} & G_{\mathbf{k}}^\dagger \\ G_{\mathbf{k}} & F_{-\mathbf{k}} \end{pmatrix} \begin{pmatrix} A_{\mathbf{k}} \\ A_{-\mathbf{k}}^\dagger \end{pmatrix}, \tag{21}$$

where $A_{\mathbf{k}} = (a_{1\mathbf{k}}, a_{2\mathbf{k}})$ is the vector of the Dyson-Maleev

boson annihilation operator, and the subindices “1” and “2” label the two sublattices of the magnetic unit cell. $F_{\mathbf{k}}$ and $G_{\mathbf{k}}$ are 2×2 matrices and depend on the mean field parameters that were introduced as boson bilinears. The quadratic spin wave Hamiltonian is diagonalized by the standard Bogoliubov transformation $Q_{\mathbf{k}}$ [34],

$$\begin{pmatrix} B_{\mathbf{k}} \\ B_{-\mathbf{k}}^\dagger \end{pmatrix} = Q_{\mathbf{k}} \begin{pmatrix} A_{\mathbf{k}} \\ A_{-\mathbf{k}}^\dagger \end{pmatrix}, \tag{22}$$

where $B_{\mathbf{k}} = (b_{1\mathbf{k}}, b_{2\mathbf{k}})$, and $Q_{\mathbf{k}}$ is a 4×4 matrix. From the ground state of the quadratic spin-wave Hamiltonian, we evaluate the mean-field boson bilinears ($\langle a_i^\dagger a_i \rangle$, $\langle a_i^\dagger a_j \rangle$, $\langle a_i^\dagger a_i^\dagger \rangle$, and $\langle a_i^\dagger a_j^\dagger \rangle$). As the spin-wave Hamiltonian depends on these boson bilinears, so we solve for them self-consistently by an iteration method.

The quantum correction is evaluated by

$$\begin{aligned}
\delta m = \langle a_i^\dagger a_i \rangle &= \frac{1}{N} \sum_i \langle a_i^\dagger a_i \rangle \\
&= \frac{1}{2} \left\{ \frac{1}{N} \sum_{\mathbf{k}} \sum_{i=1}^2 [Q_{\mathbf{k}}^\dagger Q_{\mathbf{k}}]_{ii} - 1 \right\},
\end{aligned} \tag{23}$$

where N is the number of lattice sites and we have used the simple fact that the state in region III is invariant under the combined operation of time reversal and the translation T_2 . If $\delta m > S$, the quantum fluctuation is very strong and melts the magnetic order.